Magnetodielectric coupling and multi-blocking effect in the Ising-chain magnet Sr 2 Ca 2 CoMn 2 O 9

T. Basu, N. Sakly, A. Pautrat, F. Veillon, O. Pérez, V. Caignaert, B. Raveau, V. Hardy

Magnetodielectric coupling and multi-blocking effect in the Ising-chain magnet Sr2Ca2CoMn2O9

T. Basu, N. Sakly, A. Pautrat, F. Veillon, O. Pérez, V. Caignaert, B. Raveau, and V. Hardy

Normandie University, ENSICAEN, UNICAEN, CNRS, CRISMAT, 14000 Caen, France

ABSTRACT

We have demonstrated magnetodielectric (MD) coupling in an Ising-chain magnet Sr2Ca2CoMn2O9 via detailed investigation of ac susceptibility and dielectric constant as a function of temperature, magnetic field, and frequency. Sr2Ca2CoMn2O9 consists of spin-chains made of the regular stacking of one CoO6 trigonal prism with two MnO6 octahedra. The (Co2+–Mn4+–Mn4+) unit stabilizes a (↑↓↑) spin-state along the chains that are distributed on a triangular lattice. This compound undergoes a partially disordered antiferromagnetic transition at TN ∼ 28 K. The dielectric constant exhibits a clear peak at TN only in the presence of an external magnetic field (H ≥ 5 kOe), evidencing the presence of MD coupling, which is further confirmed by field-dependent dielectric measurements. We argue that spatial inversion symmetry can be broken as a result of exchange-striction along each spin chain, inducing uncompensated local dipoles. At low temperatures, a dipolar relaxation phenomenon is observed, bearing strong similarities to the blocking effect typical of spin dynamics in this compound. Such a spin-dipole relationship is referred to as a "multiblocking" effect, in relation to the concept of magnetodielectric "multiglass" previously introduced for related materials.

I. INTRODUCTION

Multiferroic and magnetoelectric materials have been shown to be potential systems for future device applications. Various fascinating magnetoelectric phenomena have been observed in several classes of materials, and different mechanisms have been reported to be responsible for the cross coupling between spins and dipoles. Initially, it was shown that magnetism-induced ferroelectricity can be obtained in a non-collinear magnetic structure as a result of asymmetric exchange interaction [inverse Dzyaloshinskii–Moriya (D–M) interactions].1,2 Later on, it was demonstrated that the symmetric exchange interaction from a collinear magnetic structure could also induces ferroelectricity and magnetoelectric coupling.3–5 Spin-driven ferroelectricity due to exchange-striction was reported for orthorhombic perovskites RFeO3 (R = rare-earth) with a collinear magnetic structure, on which spin–orbit coupling does not have significant role.4,6 It is now clear that exchange-striction has a dominant role in spin-dipole coupling and induced ferroelectricity for the multiferroic oxides RMn2O5 3,7 and Ising-chain magnet Ca3CoMnO6, 5 as well as in 1D-organic magnets8 showing spin-Peierls instability (dimerization due to exchange-striction). Predicted in other systems as well,9 magnetic exchange-striction is also probably responsible for spin-driven pyroelectricity in the noncollinear ferrimagnet CaBaCo4O7. 10,11 Among the multiferroic oxides, those containing Co2+ are of particular interest owing to the potentially very pronounced Ising character of this cation. Ca3CoMnO6 is the first compound where exchange-striction takes place along with a peculiar ↑↑↓↓ collinear spin structure containing Mn4+ (d3) and high spin Co2+ (d7) ions, which macroscopically generates electrical

polarization at the onset of a (short-ranged) magnetic ordering (TN ∼ 15 K).5 This oxide shows a one-dimensional Ising character of the spins, with chains of dimeric units built up of MnO6 octahedra and CoO6 trigonal prisms sharing faces. Magnetoelectric coupling and multiferroicity were also observed for the compound Lu2CoMnO6 with a (↑↑↓↓) spin structure arising from the alternation of Co2+ and Mn4+ ions located in corner-shared octahedral environments.12–16 The spin chain oxides Sr4−xCaxCoMn2O9 (x = 0–2.7) (see Refs. 17–21) have an hexagonal structure belonging to the same A3MM0 O6 family as Ca3CoMnO6, but their chains consist of trimeric units of two MnO6 octahedra sharing faces with one CoO6 trigonal prism (see Fig. 1). The title compound Sr2Ca2CoMn2O9 (x = 2) exhibits several similarities to Ca3CoMnO6 since it contains the same spins (Co2+ in prisms and Mn4+ in octahedra); it also shows Ising-chain magnetism and geometrical frustration, but it strongly differs in its magnetic ground state. Indeed, the different nature of the polyhedral units, "CoMn2" instead of "CoMn," induces different intrachain interactions. In Sr2Ca2CoMn2O9, it is necessary to take into account four exchange couplings Ji, leading to a ↑ (Co2+) ↓ (Mn4+) ↑ (Mn4+) spin structure,17 compared to 3Ji in Ca3CoMnO6, which shows the (↑↑↓↓) arrangement. Moreover, a long-range ordered (LRO) magnetic state with a clear susceptibility peak at a Néel temperature TN around 28 K is observed in Sr2Ca2CoMn2O9, unlike Ca3CoMnO6, which exhibits a substantial frequency-dependent susceptibility peak due to domain dynamics and no peak in the heat capacity at TN. In other respects, recent studies revealed single-ion magnet (SIM) features in the Sr4−xCaxCoMn2 O9 series,17–20 while these magnetic behaviors are more generally observed in molecular compounds. Therefore, the Ising-chain magnet Sr2Ca2CoMn2O9, exhibits many new interesting features, which tempted us to investigate dielectric, magnetodielectric (MD), and possible ferroelectric behavior in this system. Considering the originality of spin dynamics in this material, we have paid special attention to the dynamics of electric dipoles and compared the spin and dipolar responses over a wide range of frequencies and magnetic fields.

II. EXPERIMENTAL DETAILS

The sample was prepared by a solid-state method as described in Ref. 17. The ac magnetic susceptibility (hac = 10 Oe) was recorded as a function of temperature at various frequencies (0.01–10 kHz) and in different magnetic fields (0–80 kOe) using the AC Measurement System (ACMS) option of a commercial physical properties measurements system (PPMS, Quantum design). For dielectric measurements, electrodes were painted on the two opposite large faces of the sample [dense platelet of surface (2.0 × 3.4) mm2 and thickness 0.6 mm] with silver epoxy (Dupont 4929N) cured during one day at room temperature. The measurements were then carried out by an impedance analyzer (LCR meter, E4886A, Agilent Technologies) as a function of temperature in a large frequency range of 11.1–120 kHz and magnetic field (0–80 kOe) using a home-made cryogenic insert integrated to the PPMS. The data reported in this publication have been recorded in the E // H geometry. Measurements for the E ⊥ H geometry have given similar results in this polycrystalline material. At the low temperature of measurements, the small value of the loss tangent tan δ (T) ≤ 5 · 10−2 confirms the highly insulating nature of this system and allows us to extract the intrinsic dielectric constant.

III. RESULTS

A. Evidence of magnetodielectric coupling

The χ0 (T) and χ00(T) curves [Figs. 2(a) and 2(b), respectively] recorded at a fixed frequency of 10 kHz in the presence of various magnetic fields (0–80 kOe) confirm a previous magnetic study21 and show the significant impact of an applied magnetic field on the magnetism. In the absence of a magnetic field, χ0 exhibits a peak at TN, followed by a broad hump around 10 K

(∼Tb), which was ascribed to a “blocking” temperature,21 and then sharply falls below 10 K, while χ00 exhibits a sharp peak at 8 K and a very weak peak around 28 K. However, one can distinguish an additional feature slightly above TN on the χ0 (T) and χ00(T) curves in zerofield. It was previously shown that it is a pre-transitional regime corresponding to the formation of short-range 1D ferromagneticlike segments a few K above the long-range spin ordering.21 Under the application of a dc magnetic field of 10 kOe, TN shifts to 26 K, whereas the low temperature feature Tb remains unchanged. In a dc magnetic field of 30 kOe, a broad peak is observed around 20 K in χ0 (T) followed by a change in slope around 10 K, while χ00(T) clearly exhibits both features in form of a peak at ∼20 and ∼10 K [see Fig. 2(a)]. For a field of 50 kOe, the peak at TN shifts further to lower temperature and superimposes with the 10 K feature, as revealed by the broad bump in χ0 (T). One can state that TN continuously shifts to lower temperature with increasing magnetic field, whereas the peak position of Tb remains nearly the same. The former feature is consistent with antiferromagnetic interchain, while the latter is typical of spin blocking phenomena (for energy barriers exceeding a few tens of kelvin).17,21 The temperature evolution of the dielectric constant ε0 (T) [Fig. 2(c)] and the dielectric loss tangent tan δ (T) [Fig. 2(d)] of this oxide for nearly the same 10 kHz (actually 11.1 kHz) frequency and the same applied magnetic fields shows that the dielectric and magnetic properties are closely correlated to each other. The specific 11.1 kHz (instead of exact 10 kHz) was chosen to avoid any interference on dielectric behavior from external electrical noise. However, such a small frequency mismatch has negligible difference in the dielectric feature (peak position and magnitude), and therefore one can compare to the magnetic results at 10 kHz. In the absence of a magnetic field, ε0 slowly increases with decreasing temperature from 50 K and then sharply drops below ∼10 K (Tb) down to 2 K. The loss part tan δ is nearly constant with decreasing T and then sharply increases below ∼10 K with a peak around 7 K. Thus, ε0 and tan δ trace the feature ∼Tb, mimicking the magnetism, but do not show any peak at TN in the absence of a magnetic field, unlike χ0 (T). Under a magnetic field of 1 kOe, no peak is detected at TN as well (not shown here). In contrast, a clear peak is observed at the onset of magnetic ordering TN for both real and loss tangent parts of dielectric constant in a magnetic field of 5 kOe. It is followed by a cusp with a sharp drop below a temperature T ∼ Tb. The magnitude of dielectric constant at TN and Tb becomes stronger with increasing the magnetic field. The maximum of the dielectric constant in the higher temperature region (peak position at TN) shifts to lower temperature with increasing H, that is, ε0 and tan δ show a peak below ∼28 K for 5 kOe, which shifts to 26 K for 10 kOe, as observed in magnetism. The peak position at Tb remains nearly the same when increasing the field up to 10 kOe. In a 30 kOe magnetic field, ε0 (T) yields a clear broad peak around 20 K, in accordance with the shift of TN expected for antiferromagnetic (AFM) ordering. The peak position related to TN is shifted to lower temperature with increasing further the magnetic field and finally overlaps with the feature at Tb under a very high magnetic field (say, 80 kOe). A careful analysis of tan δ (T) reveals that two features (at TN and Tb) can be clearly distinguished for H ≤ 50 kOe, whereas only one peak is observed around 7 K for H = 80 kOe, in agreement with ac susceptibility. A one-to-one correspondence between the anomalies observed in magnetic and dielectric data is highlighted in Fig. 3, displaying the temperature dependence of magnetic susceptibility and dielectric constant at nearly the same frequency (i.e., 10 and 11.1 kHz, respectively) in 10 kOe. To further support the spin-dipole coupling, we have measured the fractional change of isothermal dielectric constant [Δε0 = [ε0 (H) − ε0 (0)]/ε0 (0)] as a function of magnetic field at different temperatures, as shown in Fig. 4. A positive MD effect is observed for all the measured temperatures, including temperatures larger than TN ∼ 28 K. It is still significant in magnitude up to 40 K and almost vanishes at 70 K. Here, it is worth noting that the magnetic

susceptibility measurements indicate that the Curie–Weiss regime of a pure paramagnetic state is reached only for T ≳ 50–60 K (see Fig. 5), a feature consistent with the persistence of short-range magnetic correlation above TN. It can be inferred that such a coupling in this intermediate temperature range is a manifestation of magneto-elastic coupling (magneto-striction effect) related to the presence of short-range magnetic correlations, as observed in many other frustrated systems, including the Ising-chain cobaltate $Ca_3Co_2O_6$. 22,23 In the ordered state T<TN, the sharp change in ε0(H) around 20 kOe corresponds to the metamagnetic transition, which originates from the field-induced breaking of the partially disordered antiferromagnetic (PDA) order (due to competition between interchain exchange coupling and Zeeman energy).17 Note that the polycrystalline nature of our samples broadens the metamagnetic transition over a wide field range.

B. Spin and dipolar dynamics in the presence of a dc magnetic field

To understand the spin and dipolar dynamics and the correlation between them, we have performed frequency-dependent ac susceptibility and dielectric measurements in 10 kOe (see Fig. 6). The main signature of frequency dependence is observed in the low temperature range (below Tb), both for magnetic susceptibility and dielectric constant which exhibit a shallow maximum followed by a marked drop upon cooling. The maximum in ε0 (T) shifts to higher temperature with increasing frequency, revealing dipolar relaxation of this system. For 10 kOe, the maximum in ε0 shifts from 10 to 15 K when increasing the frequency from 11.1 to 120 kHz [see Fig. 6(c)]. It is to be noted that the maximum in χ0 for 10 kHz exactly matches with the maximum in dielectric for the very close frequency of 11.1 kHz (see Fig. 3 for a better view). The relaxation time (τ), calculated from imaginary part of ac susceptibility and dielectric constant [i.e., χ00(T, f) and ε00(T, f), where, ε00 = ε0 × tan δ)] is plotted in Fig. 6(a) as a function of 1/T. In the high temperature limit (T ≳ 5 K), the variation has an Arrhenius form $\tau = \tau_0 \cdot \exp(\Delta/T)$, where τ0 is the pre-exponential factor, i.e., attempt time, and Δ is the activation energy. The fitting in the Arrhenius limit gives $\tau_0 = 3 \cdot 10{-}9$ s and Δ = 47 K. The fact that the relaxation times of magnetic and dielectric susceptibilities obey to the same law strongly suggests that both the spin and dipolar relaxation might arise from the same mechanism. The spin chain compounds Ca_3CoBO_6, (B = Co, Mn, Rh) also exhibit frequency-dependent spin relaxation and dipolar relaxation behavior at low T below PDA,5,22–24 and it was a categorized as a "multiglass-like" behavior, similar to "magnetoelectric multiglass" where dipolar relaxation arises due to spin-dipole coupling in a spin-glass system.25–28 In $Sr_2Ca_2CoMn_2O_9$, we have previously shown17 that the spin relaxation is driven by a blocking process typical of single-ion magnetism. In this frame, the departure from the linear law in Fig. 6(c) corresponds to the crossover toward a saturation associated with quantum tunneling at the lowest temperatures. Then, considering that the spin and dipolar relaxations seem to originate from the same underlying mechanism, we will refer to this overall phenomenon as a "multiblocking" effect. As a next step, we have tried to measure the electrical polarization via pyroelectric measurements, cooling the sample from 40 down to 5 K using different voltage poling (corresponding to a maximum electric field of 285 kV/m), with and without applied magnetic field. We were unable to detect a significant pyroelectric current and an electrical polarization. At this point, it should be noted that the polycrystalline nature of the sample can strongly affect its polar response. The statistical averaging of the local polarization in grains decreases the macroscopic polarization, and the electrical coercivity can increase due to domain wall pinning at grain boundaries and defects. These two extrinsic effects can impede an efficient poling. Another possibility to explain the absence of ferroelectric response is that a

polarization is created along each spin chain, but with opposite directions making them to cancel out as a whole.

IV. DISCUSSION

In Ca3CoMnO6, Choi et al. reported the rise of electrical polarization below 15 K (regarded as a pseudo-TN) but without an associated peak in the heat capacity and no peak either in the dielectric constant (zero-field).5 For Sr2Ca2CoMn2O9, we observe both a clear magnetic susceptibility peak at the zero magnetic field and a magnetic field-induced dielectric peak for H ≥ 5 kOe. In this compound, the frequency-dependent behavior at low temperature below PDA (T< TN under different magnetic fields. Figure 8(a) represents the PDA state in the zero-field limit. Figure 8(b) illustrates the "moderate field" regime (0 < H < 20 kOe), i.e., below the metamagnetic transition. Two-thirds of the chains remain antiparallel to each other, while the incoherent chains are progressively polarized along the direction of the applied magnetic field. This yields unbalance between the up and down ↑↓↑ units along these chains, which makes both χ0 and ε0 to increase as the field is increased. The TN is still marked by a peak in magnetic χ0 and dielectric susceptibility ε0 , whose position shifts to lower values as H is increased as typically observed for an AFM transition (Fig. 2). In a strictly zerofield, the spin randomness along the incoherent chains must lead to an intrachain compensation of the dipoles associated with the exchange-striction mechanism, a feature that can explain the absence of detectable anomaly in ε0 (T). Applying a dc field allows us to partly polarize the spins along these chains, creating a most favorable direction that should be reflected on the dipoles system, inducing a non-zero overall dielectric response. Note that another role of the dc field is to counterbalance (via Zeeman energy) the cost in elastic energy associated with the exchange-striction mechanism, thereby favoring the stabilization of electrical dipoles. Figure 8(c) shows the "high field" regime, far above the metamagnetic transition, when all the chains are polarized along the same direction. It was previously shown that the metamagnetic transition is expected at ∼20 kOe when the field is applied along the c axis.17 For each grain of a polycrystalline sample, it is the component of the magnetic field along its c axis that must exceed this threshold value. Experimentally, one has observed that the signatures of the TN start vanishing in applied fields above ∼50 kOe.17 The broad maximum that is still present on the χ0 (T) and ε0 (T) curves in higher fields (Fig. 2) is ascribable only to the blocking effect at Tb. This field driven sequence from PDA/metamagnetic/polarized states can be directly seen on the Δε0 (H) curves at 20 and 15 K of the Fig. 4 and is responsible for the S shape and shows consistently the saturation of the MD effect at large field. Interestingly, at the lowest temperatures (T ≤ 10 K), the blocking effect takes place, and it yields a continuous increase of the MD response as the field is increased, without a trend of saturation (at least up to our limit of 80 kOe).

V. CONCLUSION

In summary, we have investigated the magnetodielectric properties of the Ising-chain magnet Sr2Ca2CoMn2O9 through frequency-dependent ac susceptibility and a dielectric constant in the presence of different magnetic fields as a function of temperature. A direct coupling between spin dynamics and dipole dynamics is evidenced by the same time scales measured in the dipolar relaxation and spin relaxation below PDA, which is attributed to the "multiblocking" effect. We discuss and argue on an exchange-striction origin of the magnetodielectric coupling in this exciting compound.

SUPPLEMENTARY MATERIAL

In the supplementary material, we describe the possible magnetic ground state and origin of exchange-striction, which is responsible for creating a local dipole and the possibility of ferroelectric polarization.

ACKNOWLEDGMENTS

We would like to thank Laurence Hervé (CRISMAT) for her work on the sample synthesis as well as acknowledge the ANR (No. ANR-16-CE08-0023) and the Région Normandie (Ph.D. thesis of N.S.) for their financial support. DATA AVAILABILITY The data that support the findings of this study are available within the article and its supplementary material.

REFERENCES

1 Y. Tokura, S. Seki, and N. Nagaosa, "Multiferroics of spin origin," Rep. Prog. Phys. 77(7), 076501 (2014).

2 T. Kimura, T. Goto, H. Shintani, K. Ishizaka, T. Arima, and Y. Tokura, "Magnetic control of ferroelectric polarization," Nature 426(6962), 55–58 (2003).

3 L. C. Chapon, P. G. Radaelli, G. R. Blake, S. Park, and S.-W. Cheong, "Ferroelectricity induced by acentric spin-density waves in YMn2O5," Phys. Rev. Lett. 96(9), 097601 (2006).

4 I. A. Sergienko, C. Şen, and E. Dagotto, "Ferroelectricity in the magnetic E-phase of orthorhombic perovskites," Phys. Rev. Lett. 97(22), 227204 (2006).

5 Y. J. Choi, H. T. Yi, S. Lee, Q. Huang, V. Kiryukhin, and S.-W. Cheong, "Ferroelectricity in an Ising chain magnet," Phys. Rev. Lett. 100(4), 047601 (2008).

6 Y. Tokunaga, S. Iguchi, T. Arima, and Y. Tokura, "Magnetic-field-induced ferroelectric state in DyFeO3," Phys. Rev. Lett. 101(9), 097205 (2008).

7 G. Yahia, F. Damay, S. Chattopadhyay, V. Balédent, W. Peng, E. Elkaim, M. Whitaker, M. Greenblatt, M.-B. Lepetit, and P. Foury-Leylekian, "Recognition of exchange striction as the origin of magnetoelectric coupling in multiferroics," Phys. Rev. B 95(18), 184112 (2017).

8 F. Kagawa, S. Horiuchi, M. Tokunaga, J. Fujioka, and Y. Tokura, "Ferroelectricity in a one-dimensional organic quantum magnet," Nat. Phys. 6(3), 169–172 (2010).

9 M. Pregelj, O. Zaharko, A. Zorko, Z. Kutnjak, P. Jeglič, P. J. Brown, M. Jagodič, Z. Jagličić, H. Berger, and D. Arčon, "Spin amplitude modulation driven magnetoelectric coupling in the new multiferroic FeTe2O5Br," Phys. Rev. Lett. 103(14), 147202 (2009).

10K. Singh, V. Caignaert, L. C. Chapon, V. Pralong, B. Raveau, and A. Maignan, "Spin-assisted ferroelectricity in ferrimagnetic CaBaCo4O7," Phys. Rev. B 86(2), 024410 (2012).

11V. Caignaert, A. Maignan, K. Singh, C. Simon, V. Pralong, B. Raveau, J. F. Mitchell, H. Zheng, A. Huq, and L. C. Chapon, "Gigantic magnetic-field-induced polarization and magnetoelectric coupling in a ferrimagnetic oxide CaBaCo4O7," Phys. Rev. B 88(17), 174403 (2013).

12N. Lee, H. Y. Choi, Y. J. Jo, M. S. Seo, S. Y. Park, and Y. J. Choi, "Strong ferromagnetic-dielectric coupling in multiferroic Lu2CoMnO6 single crystals," Appl. Phys. Lett. 104(11), 112907 (2014.

13S. Chikara, J. Singleton, J. Bowlan, D. A. Yarotski, N. Lee, H. Y. Choi, Y. J. Choi, and V. S. Zapf, "Electric polarization observed in single crystals of multiferroic Lu2MnCoO6," Phys. Rev. B 93(18), 180405 (2016).

14J. Blasco, J. García, G. Subías, J. Stankiewicz, J. A. Rodríguez-Velamazán, C. Ritter, J. L. García-Muñoz, and F. Fauth, "Magnetoelectric and structural properties of Y2CoMnO6: The role of antisite defects," Phys. Rev. B 93(21), 214401 (2016).

15S. Yáñez-Vilar, E. D. Mun, V. S. Zapf, B. G. Ueland, J. S. Gardner, J. D. Thompson, J. Singleton, M. Sánchez-Andújar, J. Mira, N. Biskup, M. A. Señarís-Rodríguez, and C. D. Batista, "Multiferroic behavior in the doubleperovskite Lu2MnCoO6," Phys. Rev. B 84(13), 134427 (2011).

16V. S. Zapf, B. G. Ueland, M. Laver, M. Lonsky, M. Pohlit, J. Müller, T. Lancaster, J. S. Möller, S. J. Blundell, J. Singleton, J. Mira, S. Yañez-Vilar, and M. A. Señarís-Rodríguez, "Magnetization dynamics and frustration in the multiferroic double perovskite Lu2MnCoO6," Phys. Rev. B 93(13), 134431 (2016).
17M. M. Seikh, V. Caignaert, O. Perez, B. Raveau, and V. Hardy, "Single-ion and single-chain magnetism in triangular spin-chain oxides," Phys. Rev. B 95(17), 174417 (2017).

18K. Boulahya, M. Parras, J. M. González-Calbet, and J. L. Martínez, "Synthesis, structural characterization, and magnetic study of Sr4Mn2CoO9," Chem. Mater. 15(18), 3537–3542 (2003.

19K. Boulahya, M. Hernando, M. Parras, and J. M. González-Calbet, "New stabilized phases in the Sr/Ca–Mn–Co–O system: Structural–magnetic properties relationship," J. Mater. Chem. 17(16), 1620–1626 (2007).

20M. M. Seikh, V. Caignaert, O. Perez, B. Raveau, and V. Hardy, "Interplay between single-ion magnetism, single-chain magnetism and long-range ordering in the spin chain oxides Sr4−xCaxMn2CoO9," J. Mater. Chem. C 6(13), 3362–3372 (2018).

21V. Hardy, V. Caignaert, O. Pérez, L. Hervé, N. Sakly, B. Raveau, M. M. Seikh, and F. Damay, "Pretransitional short-range ordering in a triangular lattice of Ising spin chains," Phys. Rev. B 98(14), 144414 (2018).

22T. Basu, K. K. Iyer, P. L. Paulose, and E. V. Sampathkumaran, "Dielectric anomalies and magnetodielectric coupling behavior of single crystalline Ca3Co2O6, a geometrically frustrated magnetic spin-chain system," J. Alloys Compd. 675, 364–369 (2016).

23T. Basu, K. K. Iyer, K. Singh, and E. V. Sampathkumaran, "Novel dielectric anomalies due to spin-chains above and below Néel temperature in Ca3Co2O6," Sci. Rep. 3, 3104 (2013).

24T. Basu, K. K. Iyer, K. Singh, K. Mukherjee, P. L. Paulose, and E. V. Sampathkumaran, "Anisotropic magnetodielectric coupling behavior of Ca3Co1.4Rh0.6O6 due to geometrically frustrated magnetism," Appl. Phys. Lett. 105(10), 102912 (2014).

25V. V. Shvartsman, S. Bedanta, P. Borisov, W. Kleemann, A. Tkach, and P. M. Vilarinho, "(Sr,Mn)TiO3: A magnetoelectric multiglass," Phys. Rev. Lett. 101(16), 165704 (2008).

26D. Choudhury, P. Mandal, R. Mathieu, A. Hazarika, S. Rajan, A. Sundaresan, U. V. Waghmare, R. Knut, O. Karis, P. Nordblad, and D. D. Sarma, "Near-room-temperature colossal magnetodielectricity and multiglass properties in partially disordered La2NiMnO6," Phys. Rev. Lett. 108(12), 127201 (2012).

27K. Singh, A. Maignan, C. Simon, V. Hardy, E. Pachoud, and C. Martin, "The spin glass delafossite CuFe0.5V0.5O2: A dipolar glass?," J. Phys.: Condens. Matter 23(12), 126005 (2011).

28S. Sharma, T. Basu, A. Shahee, K. Singh, N. P. Lalla, and E. V. Sampathkumaran, "Multiglass properties and magnetoelectric coupling in the uniaxial anisotropic spin-cluster-glass Fe2TiO5," Phys. Rev. B 90(14), 144426 (2014).

29Y. Zhang, H. J. Xiang, and M.-H. Whangbo, “Interplay between Jahn-Teller instability, uniaxial magnetism, and ferroelectricity in Ca3CoMnO6,” Phys. Rev. B 79(5), 054432 (2009).

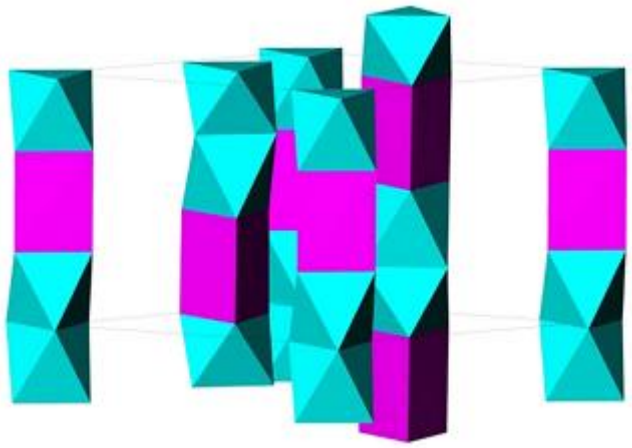

FIG. 1. Schematic structure of the stoichiometric spin chain oxide Sr2Ca2CoMn2O9. The chains distributed on a triangular network are built up of face sharing CoO6 trigonal prisms (magenta) and MnO6 octahedra (cyan). Sr and Ca distributed between chains are omitted for the sake of clarity.

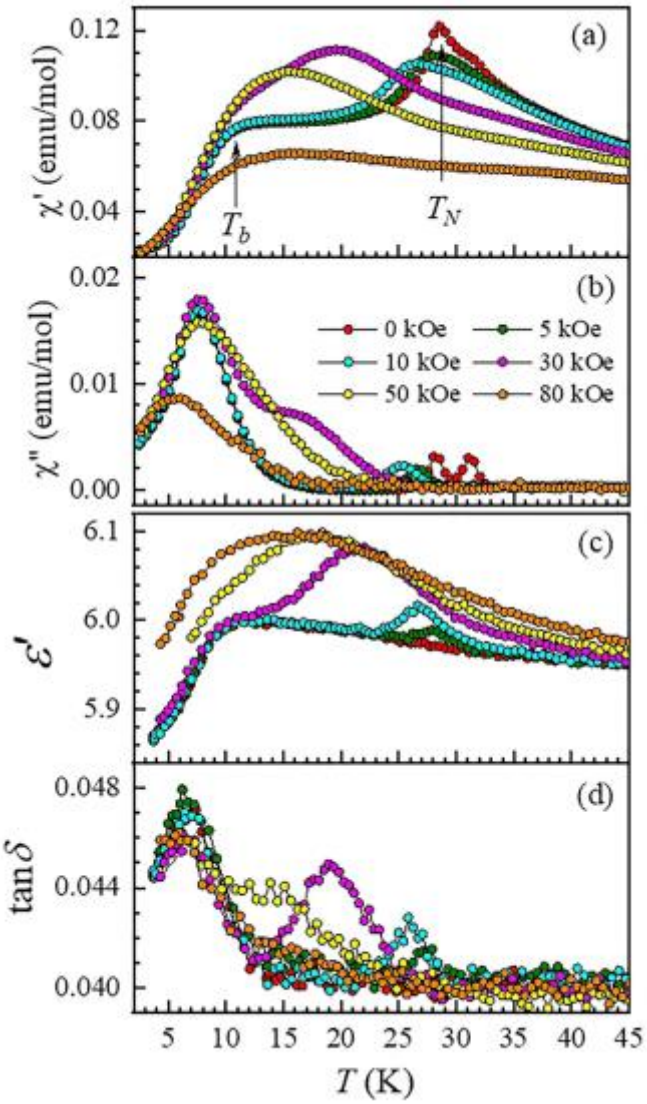

FIG. 2. Real (a) and imaginary (b) parts of ac susceptibility as a function of temperature for various fields from 0 to 80 kOe and a fixed frequency of 10 kHz. (c) and (d) are the real part and loss tangent of dielectric constant, for the same fields and for a fixed frequency of 11.1 kHz, respectively. The arrows mark the PDA transition at TN and the beginning of the blocking process at Tb, in the case of zero-field.

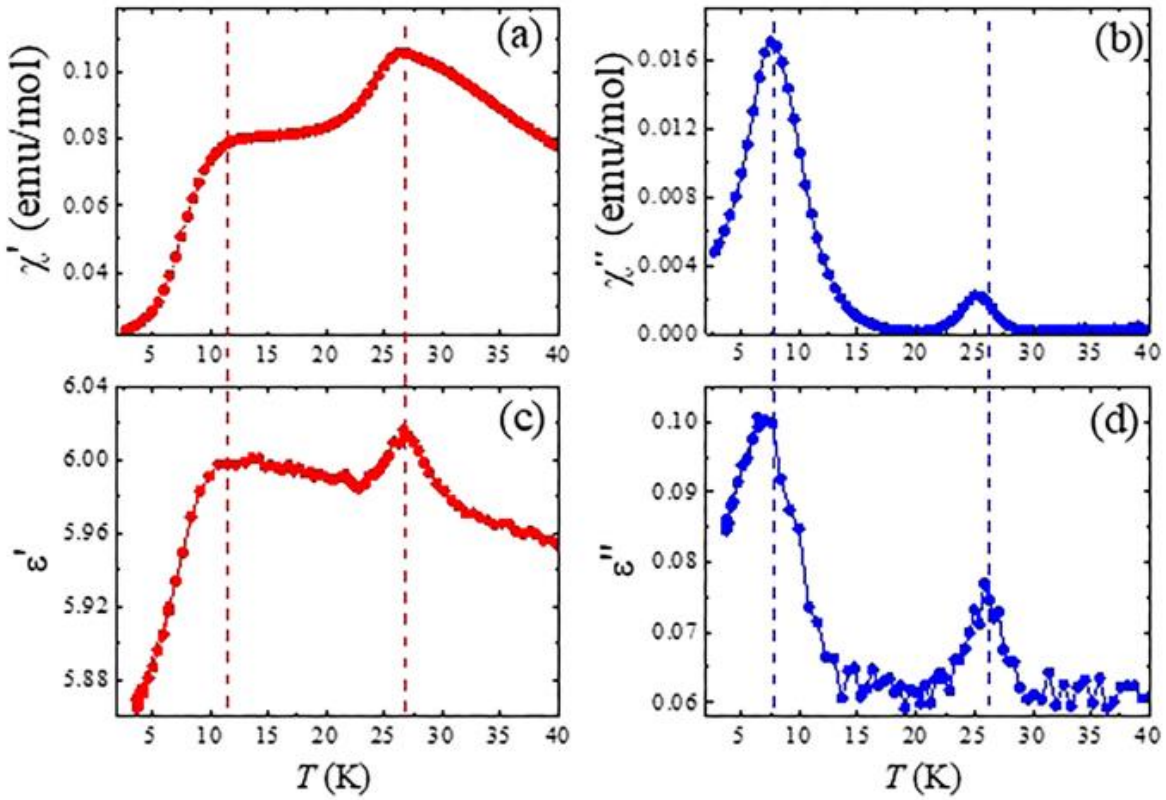

FIG. 3. In-phase (a) and out-of-phase (b) magnetic susceptibility recorded in 1 T at a frequency of 10 kHz. In-phase (c) and out-of-phase (d) dielectric constant recorded in the same magnetic field and at a very close frequency (11.1 kHz). The dashed lines show the correspondences between the magnetic and dielectric data.

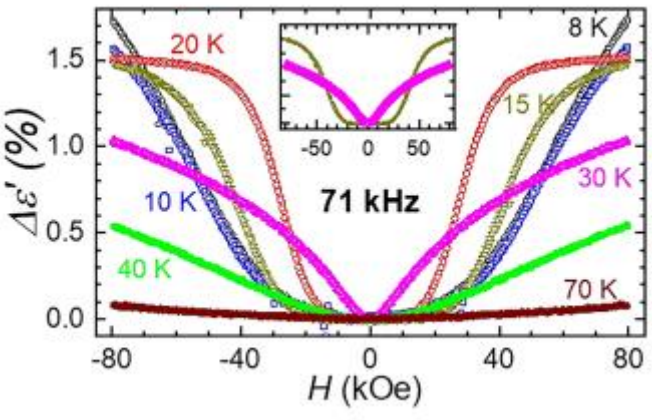

FIG. 4. Fractional change of dielectric constant as a function of magnetic field at selected temperatures and a fixed frequency of 71 kHz. The inset is an enlargement of Δε0 vs H at 15 and 30 K in order to highlight the change of shape around 20 kOe.

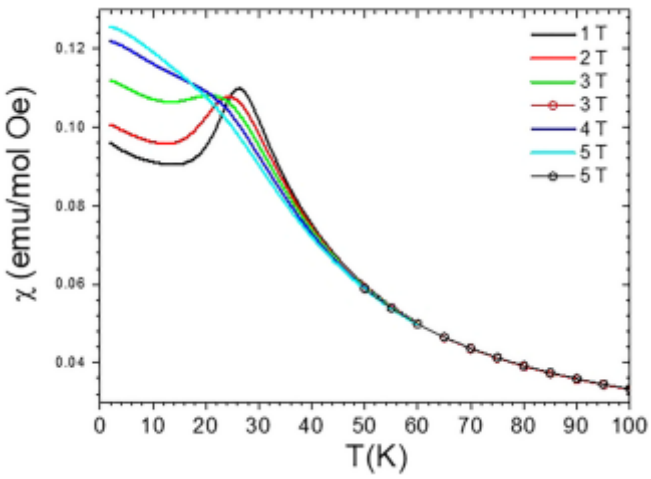

FIG. 5. dc-susceptibility curves (M/H) recorded in field cooled cooling (FCC) modes, in which the specimen is cooled under application of a magnetic field from a paramagnetic region (100 K), and data are taken in cooling down to 2 K for a series of magnetic fields. A genuine paramagnetic behavior is recovered only at T ∼ 50–60 K, i.e., significantly above the Néel temperature. dc-susceptibility curves (M/H) recorded in the field cooled cooling (FCC) mode, for selected values of the magnetic field. In the FCC mode, the measurements take place upon cooling the sample in the applied magnetic field, from the paramagnetic regime (100 K) down to 2 K. One observes that a genuine paramagnetic behavior (i.e., superimposition of all these curves) is only observed above T ∼ 50–60 K, i.e., significantly above the Néel temperature (TN ∼ 28 K)

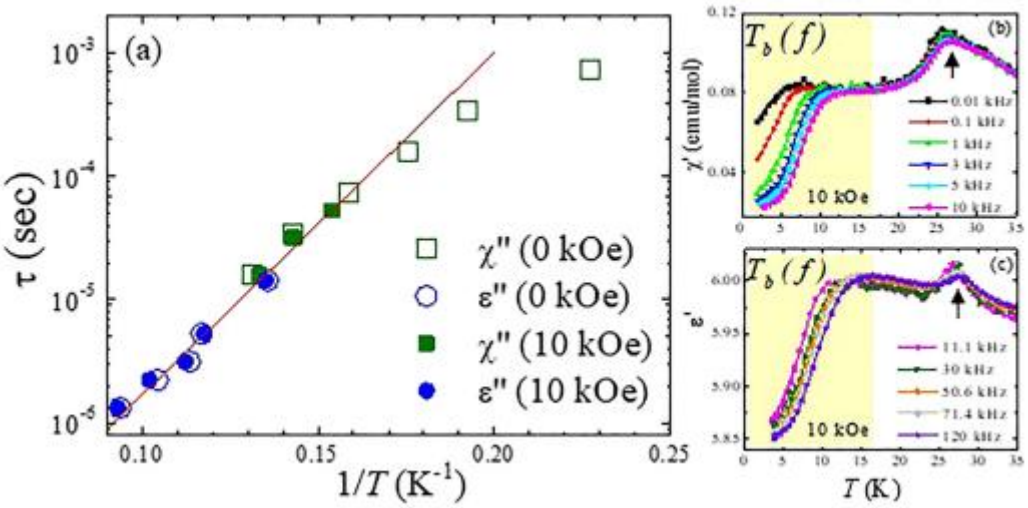

FIG. 6. Panel (a) reports the relaxation times derived from the maxima of χ00(T, f) and ε00(T, f) in both zero-field and 1 T. The red line is a fitting of the high-T part of these data to an Arrhenius law [τ = τ0 · exp(Δ/T)] leading to Δ ∼ 47 K and τ0∼ 3 · 10−9 s. Panels (b) and (c) display the in-phase magnetic susceptibility and dielectric constant measured in 1 T at various frequencies. The yellow boxes highlight the T-range over which the blocking effect takes place (starting below a frequency-dependent blocking temperature Tb). The peak at higher temperature marks the TN whose position is virtually frequency-independent.

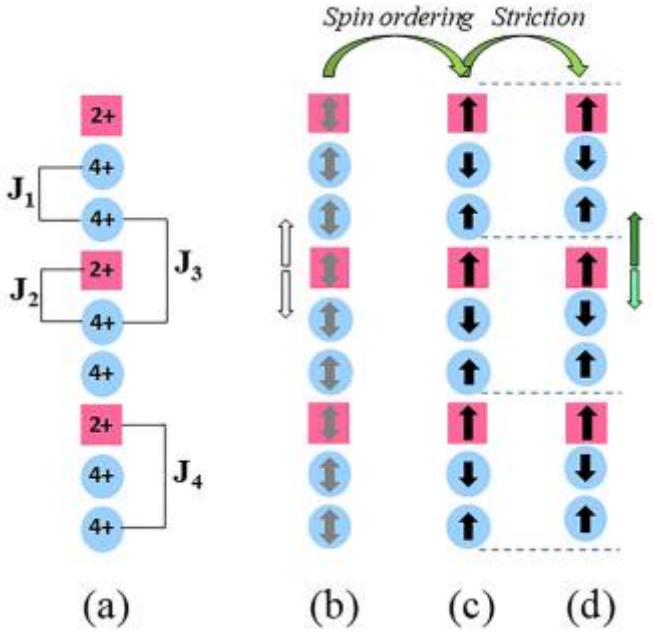

FIG. 7. Schematic representation of the alternation of Co2+ and Mn4+ along the chains. Panel (a) highlights the four types of coupling that must be taken into account. Panel (b) corresponds to the paramagnetic state; the spins are not ordered and the electric dipole between Co2+ and Mn4+ cancel each other out (white arrows). (c) Spin ordering taking place for two-thirds of the chains below TN. (d) Exchange-striction accompanying the spin ordering (see text), which induces unbalance between the electric dipoles around each Co2+ (green arrows). This yields the appearance of a net polarization along the chain.

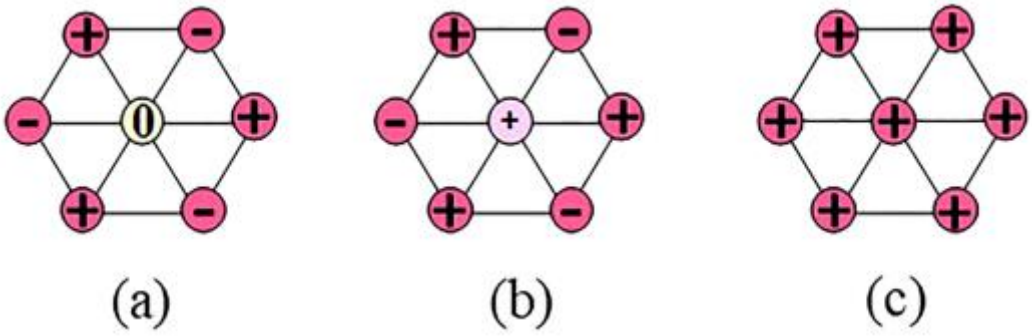

FIG. 8. Top views of the triangular chain lattice, for various regimes of applied field, at T< H < 20 kOe) tend to polarize the incoherent chains without affecting the antiferromagnetic coupling between the + and the − chains; (c) High fields (H 20 kOe) can break the antiferromagnetic interchain coupling, leading to full polarization of all the chains (in a polycrystalline sample, this regime is reached progressively, depending on the orientation of the c axis of each grain with respect to the direction of the applied field)